applied sciences

MDPI

Article

A Proposed Soft Computing Model for Ultimate Strength Estimation of FRP-Confined Concrete Cylinders

Reza Kamgar [1], Hosein Naderpour [2], Houman Ebrahimpour Komeleh [3], Anna Jakubczyk-Gałczyńska [4,*] and Robert Jankowski [4]

1 Department of Civil Engineering, Shahrekord University, Shahrekord 8818634141, Iran; kamgar@sku.ac.ir
2 Faculty of Civil Engineering, Semnan University, Semnan 98 23, Iran; naderpour@semnan.ac.ir
3 Department of Civil Engineering, Shahid Bahonar University of Kerman, Kerman 7616913439, Iran; hek2006@gmail.com
4 Faculty of Civil and Environmental Engineering, Gdansk University of Technology, 80-233 Gdansk, Poland; jankowr@pg.edu.pl
* Correspondence: annjakub@pg.edu.pl

Received: 19 January 2020; Accepted: 28 February 2020; Published: 4 March 2020

Abstract: In this paper, the feed-forward backpropagation neural network (FFBPNN) is used to propose a new formulation for predicting the compressive strength of fiber-reinforced polymer (FRP)-confined concrete cylinders. A set of experimental data has been considered in the analysis. The data include information about the dimensions of the concrete cylinders (diameter, length) and the total thickness of FRP layers, unconfined ultimate concrete strength, ultimate confinement pressure, ultimate tensile strength of the FRP laminates and the ultimate concrete strength of the concrete cylinders. The confined ultimate concrete strength is considered as the output data, while other parameters are considered as the input data. These parameters are mostly used in existing FRP-confined concrete models. Soft computing techniques are used to estimate the compressive strength of FRP-confined concrete cylinders. Finally, a new formulation is proposed. The results of the proposed formula are compared to the existing methods. To verify the proposed method, results are compared with other methods. The results show that the described method can forecast the compressive strength of FRP-confined concrete cylinders with high precision in comparison with the existing formulas. Moreover, the mean percentage of error for the proposed method is very low (3.49%). Furthermore, the proposed formula can estimate the ultimate compressive capacity of FRP-confined concrete cylinders with a different type of FRP and arbitrary thickness in the initial design of practical projects.

Keywords: FRP; soft computing; compressive strength; confined concrete; artificial neural network

1. Introduction

A combination of high-strength fibers and matrix leads to the construction of a fiber-reinforced polymer (FRP). The primary role of the matrix is to bind these fibers together to construct structural shapes. Four common types of fibers (i.e., aramid, carbon, glass, and high-strength steel) and also two standard matrices exist (i.e., epoxies and esters) [1,2]. A new area has been opened in the civil engineering field due to the beneficial properties of FRP in the repair and rehabilitation of existing structures. The FRP can create a continuous confinement action for the concrete member, and can also increase the corrosion resistance of members [3]. Hereby, FRPs are popularly used to repair or retrofit the reinforcing frame members [4–10]. Studies on the behavior of FRP and FRP-confined concrete have advanced rapidly in recent years [11]. There are a lot of publications proposing a formula

for FRP-confined concrete [12–19]. These proposed formulas are usually based on the Richard et al. method [20].

Nowadays, the use of artificial neural networks, Bayesian networks and neuro-fuzzy systems has a special place in engineering solutions, including FRP-strengthened concrete structures, structural optimization, water resource management, vibration control, bridge engineering, etc. [11,21–37]. In the study of vibrations in buildings, e.g., caused by earthquakes, the search for alternative solutions is also underway (see [38–41], for example).

An artificial neural network (ANN) was used by Lee and Lee [42] to estimate the shear strength of FRP-reinforced concrete flexural members. Sobhani et al. [43] used ANN, adaptive neuro-fuzzy inference system (ANFIS) and regression analysis to predict the compressive strength of no-slump concrete. Cheng and Cao [44] predicted the shear strength of reinforced concrete deep beams using evolutionary multivariate adaptive regression splines. In addition, the M5 model tree, used by Behnood et al. [45], is capable of predicting the elastic modulus of recycled aggregate concrete. Ebrahimpour Komleh and Maghsoudi [46] proposed a new formulation to estimate the curvature ductility factor for FRP-reinforced high-strength concrete beams using ANFIS and multiple regression methods. The ANFIS model was also used by Gu and Oyadiji [47] to control a multi-degree of freedom structures equipped with an MR damper. The ANFIS and ANN models were applied by Amini and Moeini [48] to compare results obtained for the shear strength of reinforced concrete beams with building codes. The strength of FRP connections using the backpropagation neural network was studied by Mashrei et al. [49]. The deflection of high-strength self-compacting concrete deep beams was studied by Mohammadhassani et al. applying ANFIS [50]. Nehdi and Nikopour [51] used the genetic algorithm to predict the shear capacity of reinforced concrete beams reinforced with FRP sheets.

Currently, seawater and sea sand concrete is also becoming popular due to the shortage of resources and, therefore, many researchers have focused their studies on these types of materials [52–54]. Some mechanical properties of FRP-confined concrete columns made of sea sand and seawater were studied by Li et al. [52]. They presented some theoretical models for hoop stress and strain relations and axial compression–strain relations. Zhou et al. [54] experimentally considered the effects of a chloride environment on the mechanical performance and durability of FRP-confined concrete columns made of seawater.

In this paper, the feed-forward backpropagation neural network (FFBPNN) method has been used to estimate the ultimate compressive capacity of FRP-confined concrete cylinders. For this purpose, a set of previously published and available experimental data (281 instances) for concrete made of ordinary sand has been collected for training and testing. Finally, a new formulation has been proposed to estimate the ultimate compressive capacity of FRP-confined concrete cylinders. It should be noted that the correlation coefficient of the proposed formula is equal to 0.9809, which shows a good agreement with the actual values. A comparison has been performed between the results obtained by FFBPNN and the results of the other existing models to demonstrate the ability of the proposed method. The results show that the values of the mean percentage of error (3.49%), root mean square error (3.99), and average absolute error (0.035) for the proposed method are less than other studied methods. It means that, for the proposed formula, more than 96% of the simulated results are entirely consistent with the experimental results, and also that the proposed method is very accurate compared to other existing methods. Furthermore, it is shown that the FFBPNN is a formula that can be used for all types of FRP (carbon, aramid, and glass). The proposed method can be easily employed using a calculator with high precision while, in the case of neuro-fuzzy, neural network and other known methods, a computer and sophisticated software are usually needed.

2. Research Objectives

Generally, ANNs have been used in applied science and engineering problems, because of their positive features. These features can be summarized as: (I) ability to handle the uncertainties, (II) ability to find the existing sensitivity and, finally, (III) proposing a mathematical relationship between input

and output data. This research work addresses the following main objectives. First, the feed-forward backpropagation neural network is used to predict the compressive strength of FRP-confined concrete cylinders from a set of experimental data. For this purpose, a database of experimental data has been established based on various publications. Based on these data, the main effective parameters that have an influence on the compressive strength of FRP-confined concrete cylinders (FRPCCC) are assessed. Finally, using the feed-forward backpropagation neural network, a new formulation is proposed, and the effects of the presented formula are compared with existing models.

3. Overview of Existing Models

Some published publications offer a formula to forecast the compressive strength of FRPCCC (f'_{cc}). In these papers, certain parameters are adopted as the input parameters. These parameters include the diameter of the concrete cylinder (d), length of the concrete cylinder (L), unconfined ultimate concrete strength (f'_{co}), the thickness of FRP layer (t), ultimate confinement pressure (f_l) and ultimate tensile strength of the FRP laminate (f_f). Table 1 shows the existing formula to compute the compressive strength of FRPCCC.

Table 1. Some of the existing formulas for predicting the compressive strength of fiber-reinforced polymer-confined concrete cylinders (FRPCCC).

Author	Year	Formula	Note
Mansouri et al. [55]	2016	Neuro-fuzzy, multivariate adaptive regression splines, neural network, and M5 model tree techniques (without any proposed formula)	Nonlinear
Naderpour et al. [56]	2010	$f'_{cc} = (f'_{cc})_{chart} \times C(d) \times C(L) \times C(f'_{co}) \times C(t) \times C(f_l)$ $C(d) = -0.490\left(\frac{d}{140}\right) + 1.494$ $C(L) = 0.159\ \ln\left(\frac{L}{300}\right) + 1.009$ $C(f'_{co}) = 1.082\left(\frac{f'_{co}}{35}\right)^4 - 5.071\left(\frac{f'_{co}}{35}\right)^3 + 8.209\left(\frac{f'_{co}}{35}\right)^2 - 5.025\left(\frac{f'_{co}}{35}\right) + 1.798$ $C(t) = -0.064\left(\frac{t}{1.2}\right)^2 + 0.669\left(\frac{t}{1.2}\right) + 0.387$ $C(f_l) = -0.213\left(\frac{f_l}{1500}\right)^4 + 0.901\left(\frac{f_l}{1500}\right)^3 - 1.008\left(\frac{f_l}{1500}\right)^2 + 0.723\left(\frac{f_l}{1500}\right) + 0.604$	Nonlinear
Vintzileou and Panagiotidou [18]	2008	$f'_{cc}/f'_{co} = 1 + 2.8(f_l/f'_{co})$	Linear
Berthet et al. [12]	2006	$f'_{cc}/f'_{co} = 1 + 3.45(f_l/f'_{co})$ $\quad 20 \le f'_{co} \le 50\ (MPa)$ $f'_{cc}/f'_{co} = 1 + 0.95(f_l/f'^{1.25}_{co})$ $\quad 50 \le f'_{co} \le 200\ (MPa)$	Linear-Nonlinear
Matthys et al. [15]	2005	$f'_{cc}/f'_{co} = 1 + 2.3(f_l/f'_{co})^{0.85}$	Nonlinear
Matthys et al. [15]	2005	$f'_{cc}/f'_{co} = 1 + 2.3(f_l/f'_{co})^{0.85}$	Nonlinear
Lam and Teng [13]	2002	$f'_{cc}/f'_{co} = 1 + 2(f_l/f'_{co})$	Linear
Xiao and Wu [19]	2000	$f'_{cc}/f'_{co} = 1.1 + (4.1 - 0.75f'^{2}_{co}/E_l)(f_l/f'_{co})$	Nonlinear
Miyauchi et al. [16]	2000	$f'_{cc}/f'_{co} = 1 + 3.485(f_l/f'_{co})$	Linear
Saafi et al. [17]	1999	$f'_{cc}/f'_{co} = 1 + 2.2(f_l/f'_{co})^{0.84}$	Nonlinear
Miyauchi et al. [16]	2000	$f'_{cc}/f'_{co} = 1 + 2.98(f_l/f'_{co})$	Linear

Table 1. *Cont.*

Author	Year	Formula	Note
Spoelstra and Monti [57]	1999	$f'_{cc}/f'_{co} = 0.2 + 3(f_l/f'_{co})^{0.5}$	Second-order
Toutanji [58]	1999	$f'_{cc}/f'_{co} = 1 + 3.5(f_l/f'_{co})^{0.85}$	Nonlinear
Samaan et al. [59]	1998	$f'_{cc}/f'_{co} = 1 + 6(f_l^{0.7}/f'_{co})$	Nonlinear
Kono et al. [60]	1998	$f'_{cc}/f'_{co} = 1 + 0.0572 f_l$	Linear
Karbhari and Gao [61]	1997	$f'_{cc}/f'_{co} = 1 + 2.1(f_l/f'_{co})^{0.87}$	Nonlinear
Mander et al. [62]	1988	$f'_{cc}/f'_{co} = -1.254 - 2(f_l/f'_{co}) + 2.254(1 + 7.94 f_l/f'_{co})^{0.5}$	Second-order
Fardis and Khalili [63]	1981	$f'_{cc}/f'_{co} = 1 + 2.05(f_l/f'_{co})$	Linear
Fardis and Khalili [64]	1982	$f'_{cc}/f'_{co} = 1 + 3.7(f_l/f'_{co})^{0.85}$	Nonlinear
Richart et al. [20]	1928	$f'_{cc}/f'_{co} = 1 + 4.1(f_l/f'_{co})$	Linear

It should be noted that when a concrete cylinder is subjected to the axial compression force, the compressive strength is less than its value for the FRPCCC (see Figure 1). It means that $P_1 < P_2$.

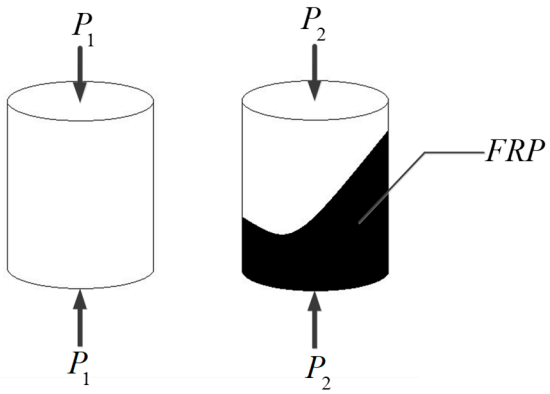

Figure 1. Two specimens (i.e., concrete cylinder and FRPCCC) subjected to the compression (an axial force).

4. Proposing a New Formulation to Predict the Compressive Strength of FRP-Confined Concrete Cylinder

In this paper, firstly, a set of experimental data is collected from the published literature [17,58,60,65–78] (see Table A1 in Appendix A). Then, the collected data are divided into input and output parameters (see Table 2).

Table 2. Input and output parameters.

Type	Parameters	Expression
Input	d (mm)	The diameter of the concrete cylinder
	L (mm)	length of the concrete cylinder
	f'_{co} (MPa)	Unconfined ultimate concrete strength
	t (mm)	The thickness of the FRP layer
	f_l (MPa)	Ultimate confinement pressure
	f_f (MPa)	The ultimate tensile strength of the CFRP laminate
Output	f'_{cc} (MPa)	Confined ultimate concrete strength

The values for minimum, maximum, mean, standard deviation, and coefficient of variation for the collected data are depicted in Table 3.

Table 3. Statistical properties for experimental data collected from the published literature.

Quantity	d (mm)	L (mm)	t (mm)	f'_{co} (MPa)	f_l (MPa)	f_f (MPa)	f'_{cc} (MPa)
Mean	133.854	272.014	0.835	42.642	15.857	2123.174	80.448
Minimum	51	102	0.089	19.4	2.33	229.762	33.8
Maximum	219	438	5.9	103	94.57	3820.359	303.6
standard deviation	27.283	58.250	1.133	17.110	12.463	1112.343	29.173
coefficient of variation	0.204	0.214	1.357	0.401	0.786	0.524	0.363

4.1. The Artificial Neural Network Model

ANNs are among the computational software methods used. The neural networks can find the existing patterns between the input and output data of experiments or simulations via training [79]. It is noteworthy that layers, neurons and weights can compose the neural networks. Here, the primary role of the weights is to relate every neuron in each layer to the neurons in other layers. Every neuron is associated with neurons in other layers by the weights. Every layer processes the input data and transfers them to the next layer. Additionally, an input layer, two or more hidden layers and an output layer compose the feed-forward neural network. A three-layer neural network is depicted in Figure 2. As mentioned in Section 3, the number of collected data is 281. These data are used for the learning, validating, and testing of ANNs. In the neural network modeling, log-sigmoid transfer functions are used and one hidden layer is selected. Firstly, all selected data are normalized based on the following equation:

$$\begin{aligned} f_{scaled} &= (0.9 - 0.1)\left(\frac{f - f_{\min}}{f_{\max} - f_{\min}}\right) + 0.1 \\ 0.1 &\le f_{scaled} \le 0.9 \end{aligned} \quad (1)$$

where f, $f_{\min}$, $f_{\max}$ and f_{scaled} are the selected parameters, their minimum and maximum values are based on Table 3 and the value of the scaled parameters, respectively. Based on Equation (1), the scaled parameters place in the range between 0.1 and 0.9, as recognized by the log-sigmoid transfer functions.

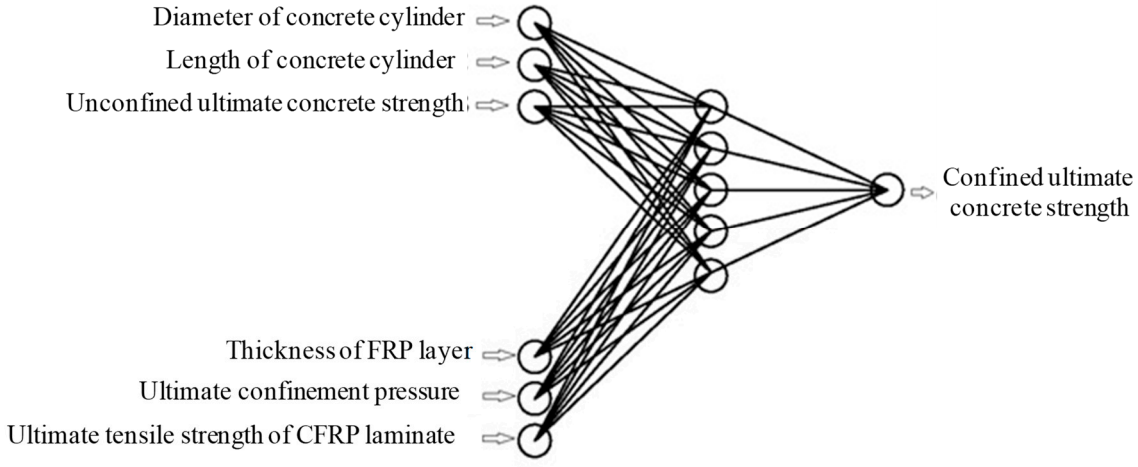

Figure 2. A three-layer artificial neural network.

The Levenberg–Marquardt algorithm is used to train randomly divided input and output vectors, which are called training (also learning), validating (also verifying) and testing datasets. Since improving the performance of the ANN model can be done by finding the optimal distribution of the datasets, various sets were analyzed. Finally, the best division was chosen, in which 70% of all data were training sets, while 15% of all data were validating and testing sets, respectively.

For this purpose, a 6:n:1 network is considered with six inputs, n hidden neurons and one output, respectively (see Figure 2). Moreover, the flowchart of the utilized ANN is depicted in Figure 3.

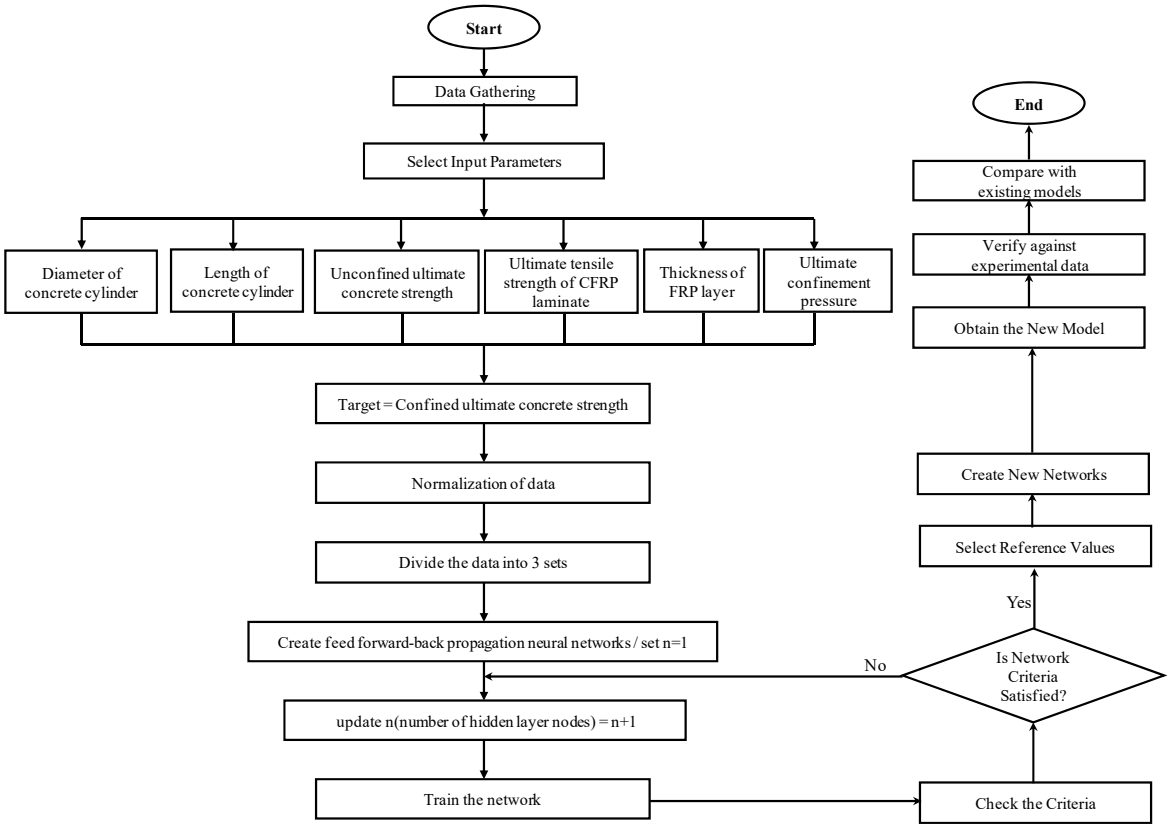

Figure 3. Flowchart of the utilized artificial neural network (ANN) for predicting the confined ultimate concrete strength.

The mean squared error (MSE) is considered as a criterion to stop the training of the networks. The MSE is defined as the average squared difference and is an important value that indicates an error between the network output and the actual value obtained from research. Therefore, when the quantity for the desired network has a minimum value, this network has a better performance. In addition, in a network, the correlation between outputs and targets is measured by regression values (R-values). The R-value is a parameter to measure the correlation between targets and outputs. These two criteria are selected to recognize which network has a better performance.

Figure 4 shows the regression values of the networks versus the different numbers of neurons in hidden layers. Furthermore, Figure 5 presents the maximum absolute value for the error of each network. From the above description and considering Figures 4 and 5, it can be concluded that a network with 15 hidden neurons had the best performance.

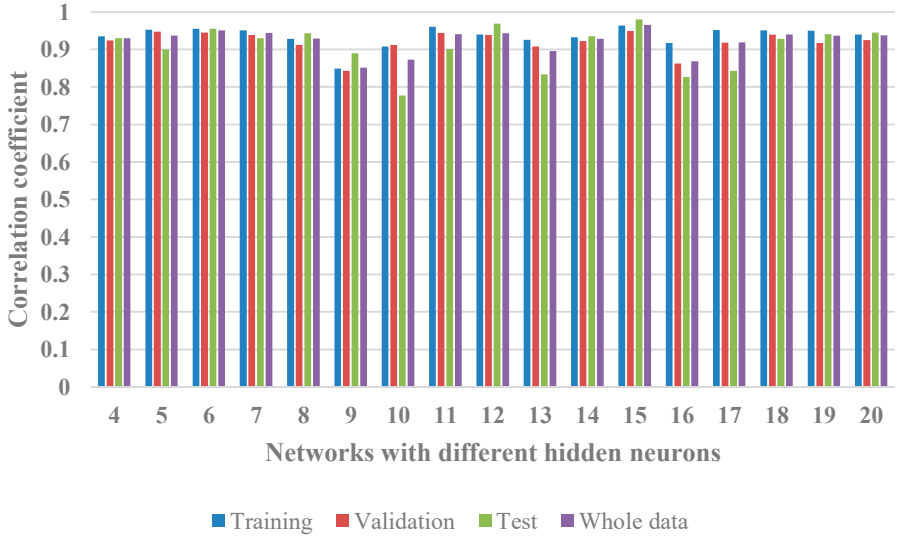

Figure 4. The correlation coefficient with different values of ANN 6:*n*:1.

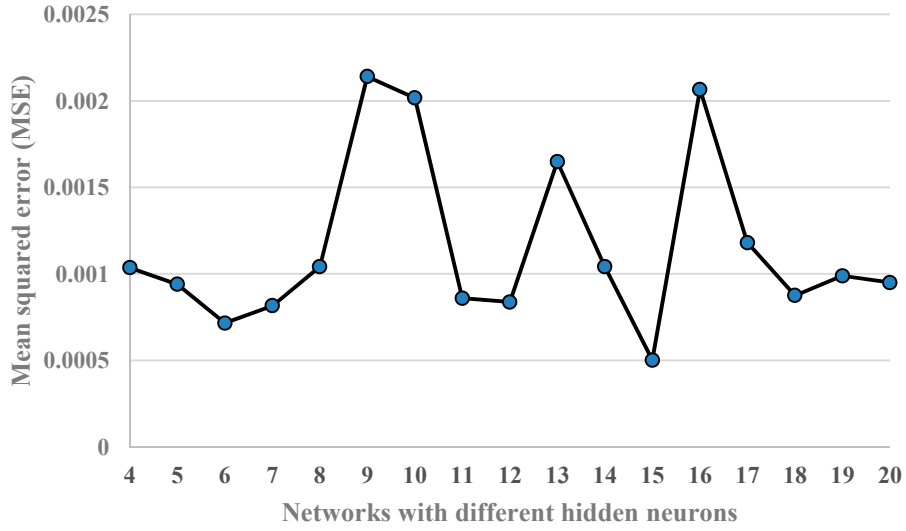

Figure 5. Mean squared error (MSE) versus some hidden-layer neurons.

After selecting a desirable network (6:15:1), the results for the training of this network are shown in Figures 6–8. It can be seen from Figure 6 that the network is well established and learned, since the values for MSE of the network begin at a large value and stop at a smaller one.

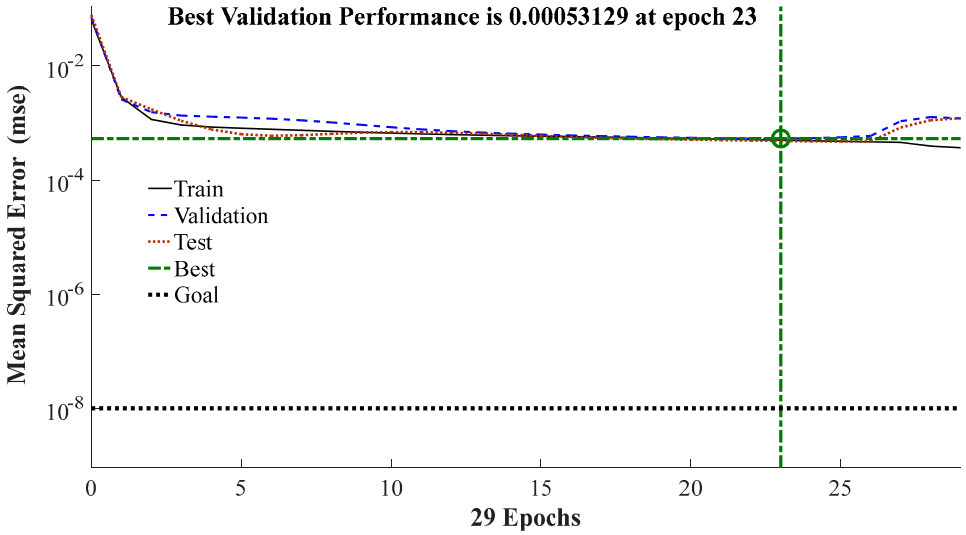

Figure 6. Performance of ANN 6:15:1.

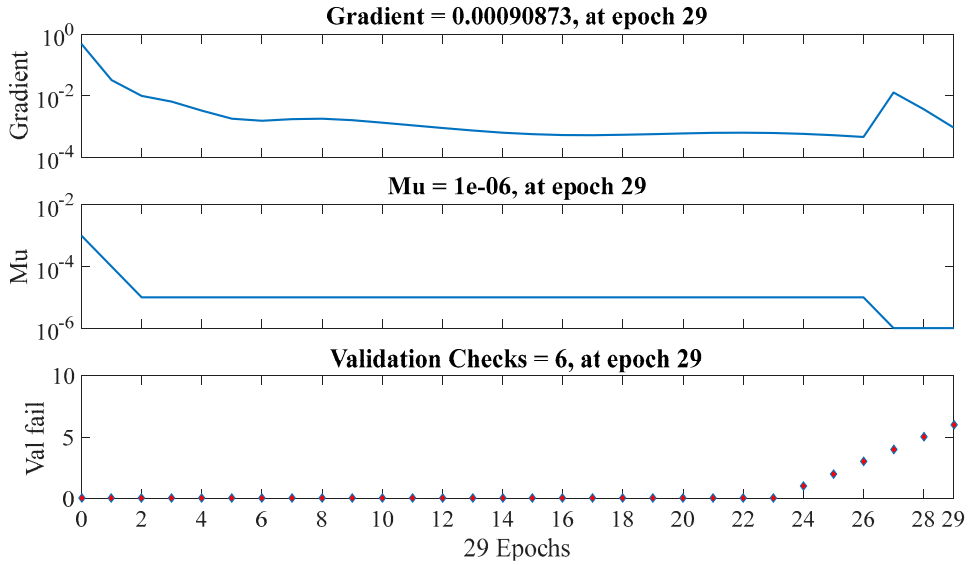

Figure 7. Training state of ANN 6:15:1.

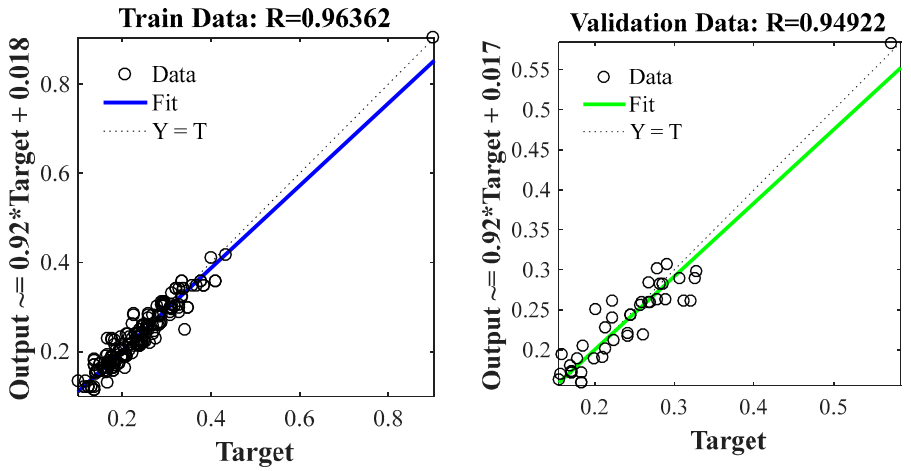

Figure 8. *Cont.*

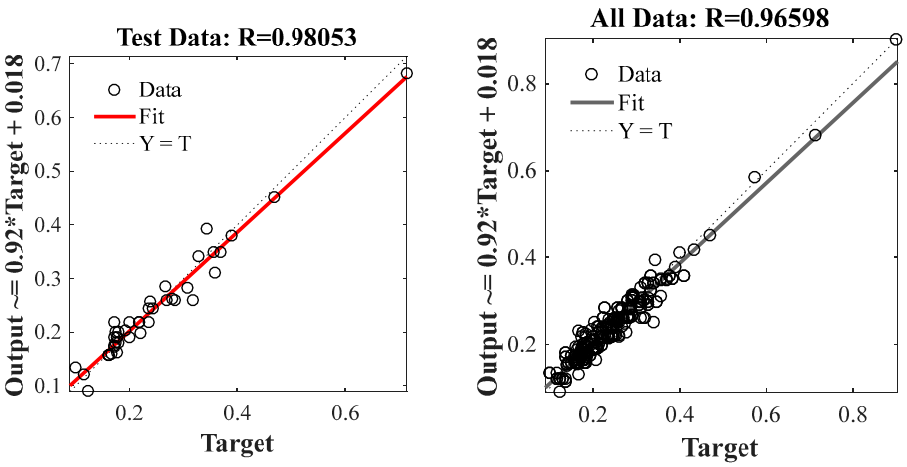

Figure 8. Regressions of training, validating, and testing datasets simulated by ANN 6:15:1.

It should be noted that the ANN technique cannot propose a formulation to predict the compressive strength of FRPCCC. Therefore, in the next section of this paper, the K-fold cross-validation technique is used to obtain a new formulation. Then, the efficiency of the proposed formula is examined.

4.2. Using a Model with a K-Fold Cross-Validation Technique in FFBPNN

In this section of the paper, a K-fold cross-validation (KFCV) technique is applied for the optimization and evaluation of the perfected ANN [80,81]. In the KFCV technique, the data are divided randomly into K folds. Then, the K-1 folds are used for training, and the last fold is used to test the neural network. In the parametric study conducted, the values for K, changing from two to five and K = 4, are considered. The process of learning and testing is conducted for all the K sections. Therefore, all the K sections contribute to the learning and testing of the ANN. This process is iterated three times for the reduction and variation of KFCV and similar distribution of data in each K. The performance of the neural network for each iteration can be computed by the percentage of correct predictions in the neural network for K folds.

In every epoch, the performance evaluation of the neural network is calculated. The curve is the correct classification factor (CCF), it is drawn for three iterations and, finally, it is averaged. In the CCF curve, after a specified epoch, the curve is saturated. Then, the optimal epoch is defined using 10% of the curve plateau. In this study, a neural network with three layers is selected for the sake of simplicity. For optimization of the ANN structure, some neurons in the hidden layer are optimized. For this purpose, the selecting criteria are considered to be the area under the CCF curve (AUCCF). Therefore, the AUCCF is measured until it reaches the optimal epoch. Hence, different neurons, from two to 13 neurons in the hidden layer, are selected and the KFCV process is repeated for the structures. Finally, the structure with the maximum efficiency can be determined by drawing the CCF and calculating the AUCCF. Figure 9 shows the AUCCF curve. As can be seen from this figure, the 6:11:1 structure with 11 neurons in the hidden layer has the highest performance with 86.6%. Figure 10 shows the CCF curve for the optimized ANN structure. As shown in this figure, the optimum epoch is 224.

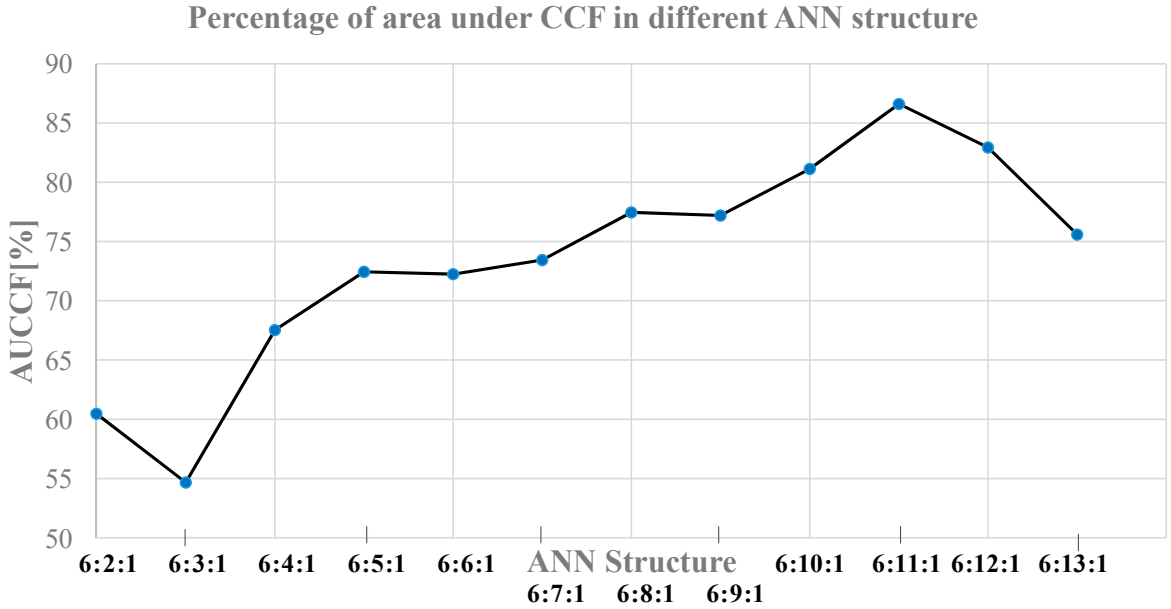

Figure 9. Area under the correct classification factor (AUCCF) curve of the neural network with different structures.

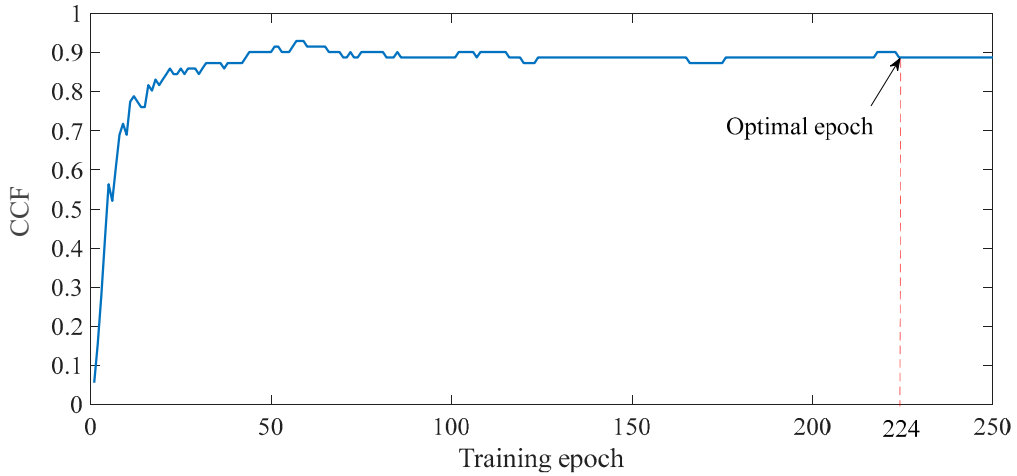

Figure 10. The CCF curve of optimized ANN structure.

Data that are predicted by the optimized ANN neural network and the training data are plotted in Figure 11. As shown in this figure, the correlation coefficient is equal to 0.9809, which confirms the performance of the optimized ANN structure.

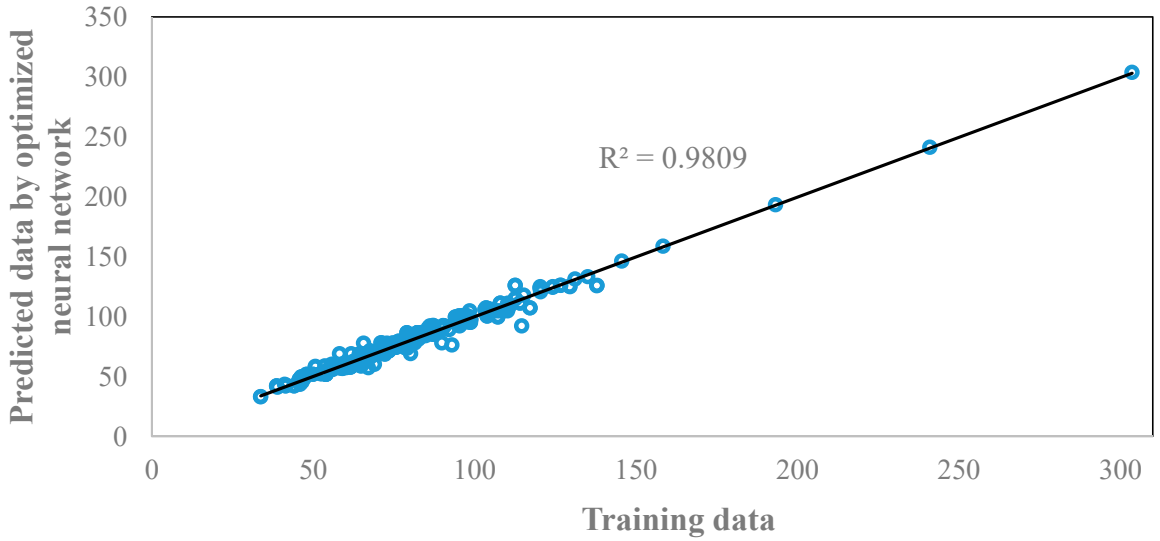

Figure 11. The correlation coefficient of the predicted data by optimized ANN structure and training data.

The Tansig and Pureline activation functions are selected for the hidden layer and the output layer, respectively. Considering the optimum structure of the neural network, weights, biases, and activation functions, a relation, such as Equation (2), could be extracted:

$$Output = \left(\frac{2}{1 + exp^{(-2\times(Input\times Iw + b_1))}} - 1\right) \times Lw + b_2 \tag{2}$$

Input, *Output*, *IW*, *LW*, b_1, and b_2 in Equation (2) are constant coefficients, which are defined as follows:

$$IW = \begin{bmatrix} -1.2007 & -0.6174 & 2.6247 & 0.3393 & -0.7012 & 1.6310 \\ 13.2928 & -16.8285 & 8.4865 & 1.3056 & -0.4213 & -7.0180 \\ -1.0486 & -0.0470 & -2.9279 & 0.5110 & -2.2153 & -0.2471 \\ -6.1496 & 3.0775 & 7.2171 & -3.7018 & 16.1829 & -15.3115 \\ 3.2838 & -0.7242 & -0.5853 & 0.0652 & 0.5304 & -1.0226 \\ -0.9033 & 0.8337 & 3.1251 & 2.2056 & 1.3875 & 2.3565 \\ -0.9161 & 0.6510 & 1.1284 & -0.1900 & 0.5996 & 0.5913 \\ 5.4701 & 1.9650 & 1.4193 & -0.8012 & -0.3120 & 1.6189 \\ -1.3924 & -1.9230 & 6.6908 & -12.3073 & 2.1772 & 1.0588 \\ -12.8275 & 14.9574 & 11.9745 & 3.8238 & -21.2448 & 23.5244 \\ 12.3926 & 10.8354 & -2.5711 & -8.0694 & 11.5337 & 0.1035 \end{bmatrix}^T$$

$$LW = \begin{bmatrix} -7.7570 & -0.1861 & 0.2698 & -0.2166 & 1.1077 & 1.2329 & 1.6244 & -0.7781 & -3.3951 & 0.1298 & -1.1472 \end{bmatrix}^T$$

$$b_1 = \begin{bmatrix} -1.7314 & 4.5025 & -3.2840 & 26.0974 & 0.7293 & 1.5696 & 1.5758 & -0.6336 & 16.9266 & 2.9547 & 17.0029 \end{bmatrix}$$

$$b_2 = -3.9606$$

$$Input = [\ d \quad L \quad t \quad f'_{co} \quad f_l \quad f_f\ ]$$

$$Output = [f'_{cc}] \tag{3}$$

5. Comparison of the Proposed Strength Model with Existing Empirical Ones

Five known models are selected [12,13,15,16,18,56] to verify the proposed formula. It must be noted that no formula has been proposed in the most recent available publication [55]. The formula proposed in this paper can be implemented in a calculator, while, in the case of the neuro-fuzzy, neural network, multivariate adaptive regression splines and M5 model tree techniques (all considered in [55]), a computer and professional programs should be used.

Figure 12 shows the values of the compressive strength of the FRPCCC obtained by the proposed and existing formula versus the experimental values. Table A1 in the Appendix section shows the experimental data that have been used to judge the ability of different methods. In fact, for all formulas,

the same data are applied to forecast the compressive strengths of the FRPCCC. Figure 12 shows that the presented formula can estimate the compressive strengths of the FRPCCC with a higher precision compared to the existing formulas.

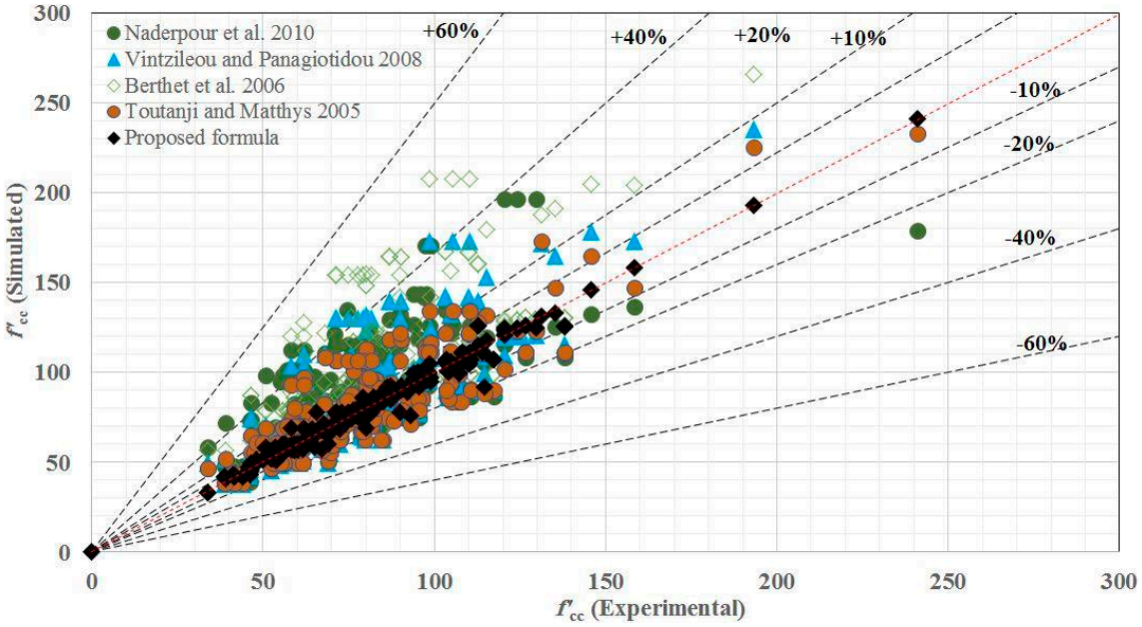

Figure 12. Comparison between simulated and experimental results for the compressive strength of FRPCCC.

The mean percentage of error, correlation coefficient, root mean square error (RMSE), and average absolute error (AAE) for the studied methods are shown in Table 4 to verify the efficiency of the proposed method. Based on this table, it should be noted that the mean percentage of error and the correlation coefficient for the proposed method are equal to 3.49% and 0.9809, respectively. Meanwhile, the corresponding values for other existing methods are equal to over 13% and 0.41, respectively. This means that, for the proposed formula, more than 96% of the simulated results are entirely consistent with the experimental ones. Furthermore, the minimum values of RMSE and AAE are obtained for the proposed formula. Therefore, it should be pointed out that the proposed formula is very accurate compared to other existing ones, for which the accuracy is lower than 85%.

Table 4. Comparison between different studied models.

Method Error	Miyauchi et al. [16]	Lam and Teng [13]	Matthys et al. [15]	Berthet et al. [12]	Vintzileou and Panagiotidou [18]	Naderpour et al. [56]	Proposed Formula
Mean percentage of error	17.77%	16.95%	13.14%	17.59%	15.42%	8.44%	3.49%
RMSE	31.83	14.96	13.95	31.20	20.64	12.86	3.99
AAE	0.28	0.15	0.14	0.25	0.18	0.11	0.035
correlation coefficients	0.6813	0.7897	0.8064	0.6835	0.7288	0.7686	0.9809

Based on Figures 11 and 12, as well as Table 4, it is evident that the proposed formula has a good agreement with the actual values. Therefore, it can be used in the practical projects to evaluate the amount of column compressive capacity reinforced by FPR sheets in the initial design. It should be noted that the collected data (see Appendix A) are for different types of FRP sheets (carbon, aramid, and glass) and the FFBPNN method has been trained and tested with these data. Therefore, the proposed

formula can estimate the ultimate compressive capacity of FRP-confined concrete cylinders with a different type of FRP and arbitrary thickness.

6. Concluding Remarks

A soft computing model for the ultimate strength estimation of FRPCCC has been proposed in this paper. A set of experimental data from the published literature has been collected and divided into input and output parameters. Firstly, the ANN model has been created and analyzed. The mean squared error and R-values have been used to verify the efficiency of the network.

The results of the analysis indicate that a network with 15 hidden neurons has the best performance. However, it should be noted that the basic ANN technique cannot propose a formulation to forecast the compressive strength of FRPCCC. Therefore, in the next step of the study, the author's improvement approach has been presented. A model with a K-fold cross-validation technique in the feed-forward backpropagation neural network has been presented. The correlation coefficient, root mean square error, mean percentage of error and average absolute error have been used to check its efficiency. The structure with 11 neurons in the hidden layer has been found to give the best performance. Finally, a comparison between the proposed formula and existing empirical ones has been conducted. To verify the proposed formula, five known models described in this paper have been selected. The results of the study show that the proposed method can estimate the compressive strengths of the FRPCCC with higher precision compared to the existing formulas. Moreover, it can be used to predict the compressive strength of FRPCCC with different types and arbitrary thicknesses of FRP (carbon, aramid, and glass). It should be noted that the mean percentage of error and the correlation coefficient for the proposed method are equal to 3.49% and 0.9809, respectively. Meanwhile, the corresponding values for other existing methods are equal to over 13% and 0.41, respectively. It means that, for the proposed formula, more than 96% of the simulated results are entirely consistent with the experimental results. Furthermore, the minimum values of RMSE and AAE have been obtained for the proposed formula. Therefore, it should be pointed out that the proposed formula is very accurate compared to other existing methods, for which the accuracy is usually lower than 85%. It should also be added that the proposed method can be easily employed using a calculator with high precision while, in the case of the neuro-fuzzy network, neural network and other known methods, a computer and sophisticated software is usually needed. Therefore, our model can be used to estimate the ultimate compressive capacity of FRP-confined concrete cylinders in the initial design of practical projects.

Finally, it should be noted that there is a lack of experimental tests on concrete cylinders made of seawater and sea sand retrofitted with FRP sheets in order to propose a formula that covers the entire region. This should be a focus in future studies.

Author Contributions: Conceptualization, R.K. and H.N.; methodology, R.K., H.N., H.E.K., A.J.-G. and R.J.; software, R.K., H.N. and H.E.K.; validation, R.K., H.N., H.E.K., A.J.-G. and R.J.; formal analysis, R.K., H.N. and H.E.K.; investigation, R.K. and H.N.; writing—original draft preparation, R.K., H.N., and H.E.K.; writing—review and editing, A.J.-G. and R.J. All authors have read and agreed to the published version of the manuscript.

Funding: This research received no external funding.

Conflicts of Interest: The authors declare no conflict of interest.

Appendix A

The collected data are indicated in Table A1.

Table A1. The collected data from experimental studies.

No.	Ref.	Fiber Type	d (mm)	L (mm)	t (mm)	f'_{co} (MPa)	f_l (MPa)	f_f (MPa)	f'_{cc} (MPa)
1	[72]	CFRP	150	300	0.11	45.2	5.2	3481	59.4
2	[72]	CFRP	150	300	0.22	45.2	10.08	3481	79.4
3	[72]	CFRP	150	300	0.11	31.2	5.04	3481	52.4
4	[72]	CFRP	150	300	0.22	31.2	10.14	3481	67.4
5	[72]	CFRP	150	300	0.33	31.2	15.31	3481	81.7
6	[72]	CFRP	100	200	0.11	51.9	7.7	3481	75.2
7	[72]	CFRP	100	200	0.22	51.9	15.15	3481	104.6
8	[72]	CFRP	100	200	0.11	33.7	7.57	3481	69.6
9	[72]	CFRP	100	200	0.22	33.7	15.39	3481	88
10	[72]	CFRP	150	300	0.11	45.2	5.2	3481	59.4
11	[60]	CFRP	100	200	0.167	34.3	12.77	3820	57.4
12	[60]	CFRP	100	200	0.167	34.3	12.85	3820	64.9
13	[60]	CFRP	100	200	0.167	32.3	12.85	3820	58.2
14	[60]	CFRP	100	200	0.167	32.3	12.77	3820	61.8
15	[60]	CFRP	100	200	0.167	32.3	12.67	3820	57.7
16	[60]	CFRP	100	200	0.334	32.3	27.69	3820	61.8
17	[60]	CFRP	100	200	0.334	32.3	35.55	3820	80.2
18	[60]	CFRP	100	200	0.334	32.3	16.4	3820	58.2
19	[60]	CFRP	100	200	0.501	32.3	38.33	3820	86.9
20	[60]	CFRP	100	200	0.501	32.3	38.27	3820	90.1
21	[60]	CFRP	100	200	0.167	34.8	12.8	3820	57.8
22	[60]	CFRP	100	200	0.167	34.8	12.67	3820	55.6
23	[60]	CFRP	100	200	0.167	34.8	12.66	3820	50.7
24	[60]	CFRP	100	200	0.334	34.8	25.4	3820	82.7
25	[60]	CFRP	100	200	0.334	34.8	25.46	3820	81.4
26	[60]	CFRP	100	200	0.501	34.8	38.38	3820	103.3
27	[60]	CFRP	100	200	0.501	34.8	38.24	3820	110.1
28	[69]	CFRP	150	300	0.117	34.9	4.08	2600	46.1
29	[69]	CFRP	150	300	0.235	34.9	3.44	1100	45.8
30	[77]	CFRP	153	306	0.36	19.4	10.77	2275	33.8
31	[77]	CFRP	153	306	0.66	19.4	19.71	2275	46.4
32	[77]	CFRP	153	306	0.9	19.4	26.87	2275	62.6
33	[77]	CFRP	153	306	1.08	19.4	32.2	2275	75.7
34	[77]	CFRP	153	306	1.25	19.4	37.32	2275	80.2
35	[77]	CFRP	153	306	0.36	49	10.68	2275	59.1
36	[77]	CFRP	153	306	0.66	49	19.77	2275	76.5
37	[77]	CFRP	153	306	0.9	49	26.85	2275	98.8
38	[77]	CFRP	153	306	1.08	49	32.3	2275	112.7
39	[75]	CFRP	100	200	0.6	42	15.21	1265	73.5
40	[75]	CFRP	100	200	0.6	42	15.21	1265	73.5
41	[75]	CFRP	100	200	0.6	42	15.15	1265	67.62
42	[75]	AFRP	150	300	1.26	43	3.82	230	47.3
43	[75]	AFRP	150	300	2.52	43	7.76	230	58.91
44	[75]	AFRP	150	300	3.78	43	11.66	230	70.95
45	[75]	AFRP	150	300	5.04	43	15.46	230	74.39
46	[70]	GFRP	100	200	0.35	32	10.63	1520	54
47	[70]	GFRP	100	200	0.35	32	10.69	1520	48
48	[70]	GFRP	100	200	0.35	32	10.63	1520	54
49	[70]	GFRP	100	200	0.35	32	10.61	1520	50
50	[70]	CFRP	100	200	0.16	37	12.2	3790	60
51	[70]	CFRP	100	200	0.16	37	12.15	3790	62
52	[70]	CFRP	100	200	0.16	37	12.13	3790	59
53	[70]	CFRP	100	200	0.16	37	12.11	3790	57
54	[76]	CFRP	150	300	0.169	25.15	4.63	2024	44.13
55	[76]	CFRP	150	300	0.169	25.15	4.61	2024	41.56
56	[76]	CFRP	150	300	0.169	25.15	4.55	2024	38.75
57	[76]	CFRP	150	300	0.338	25.15	9.11	2024	60.09
58	[76]	CFRP	150	300	0.338	25.15	9.14	2024	55.93
59	[76]	CFRP	150	300	0.338	25.15	9.19	2024	61.61
60	[76]	CFRP	150	300	0.507	25.15	13.64	2024	67

Table A1. *Cont.*

No.	Ref.	Fiber Type	d (mm)	L (mm)	t (mm)	f'_{co} (MPa)	f_l (MPa)	f_f (MPa)	f'_{cc} (MPa)
61	[76]	CFRP	150	300	0.507	25.15	13.72	2024	67.27
62	[76]	CFRP	150	300	0.507	25.15	13.72	2024	70.18
63	[76]	CFRP	150	300	0.169	47.44	4.64	2024	72.26
64	[76]	CFRP	150	300	0.169	47.44	4.61	2024	64.4
65	[76]	CFRP	150	300	0.169	47.44	4.57	2024	66.19
66	[76]	CFRP	150	300	0.338	47.44	9.12	2024	82.36
67	[76]	CFRP	150	300	0.338	47.44	9.12	2024	82.35
68	[76]	CFRP	150	300	0.338	47.44	9.08	2024	79.11
69	[76]	CFRP	150	300	0.507	47.44	13.79	2024	96.29
70	[76]	CFRP	150	300	0.507	47.44	13.74	2024	95.22
71	[76]	CFRP	150	300	0.507	47.44	13.77	2024	103.9
72	[76]	CFRP	150	300	0.169	51.84	4.62	2024	78.65
73	[76]	CFRP	150	300	0.169	51.84	4.54	2024	79.18
74	[76]	CFRP	150	300	0.169	51.84	4.57	2024	72.76
75	[76]	CFRP	150	300	0.338	51.84	9.23	2024	95.4
76	[76]	CFRP	150	300	0.338	51.84	9.16	2024	90.3
77	[76]	CFRP	150	300	0.338	51.84	9.02	2024	90.65
78	[76]	CFRP	150	300	0.507	51.84	13.77	2024	110.5
79	[76]	CFRP	150	300	0.507	51.84	13.64	2024	103.6
80	[76]	CFRP	150	300	0.507	51.84	13.65	2024	117.2
81	[76]	CFRP	150	300	0.845	51.84	22.78	2024	112.6
82	[76]	CFRP	150	300	0.845	51.84	22.87	2024	126.6
83	[76]	CFRP	150	300	0.845	51.84	22.67	2024	137.9
84	[76]	CFRP	150	300	0.169	70.48	4.53	2024	87.29
85	[76]	CFRP	150	300	0.169	70.48	4.53	2024	84.03
86	[76]	CFRP	150	300	0.169	70.48	4.53	2024	83.22
87	[76]	CFRP	150	300	0.338	70.48	9.19	2024	94.06
88	[76]	CFRP	150	300	0.338	70.48	9.14	2024	98.13
89	[76]	CFRP	150	300	0.338	70.48	9.22	2024	107.2
90	[76]	CFRP	150	300	0.507	70.48	13.7	2024	114.1
91	[76]	CFRP	150	300	0.507	70.48	13.63	2024	108
92	[76]	CFRP	150	300	0.507	70.48	13.48	2024	110.3
93	[76]	CFRP	150	300	0.169	82.13	4.75	2024	94.08
94	[76]	CFRP	150	300	0.169	82.13	5.2	2024	97.6
95	[76]	CFRP	150	300	0.169	82.13	4.98	2024	95.83
96	[76]	CFRP	150	300	0.338	82.13	10.15	2024	97.43
97	[76]	CFRP	150	300	0.338	82.13	9.14	2024	98.85
98	[76]	CFRP	150	300	0.338	82.13	9.92	2024	98.24
99	[76]	CFRP	150	300	0.507	82.13	13.59	2024	124.2
100	[76]	CFRP	150	300	0.507	82.13	13.76	2024	129.5
101	[76]	CFRP	150	300	0.507	82.13	13.42	2024	120.3
102	[65]	GFRP	102	203	1	38.99	40.75	2078	115.3
103	[65]	GFRP	102	203	1	50.51	40.75	2078	135.1
104	[65]	GFRP	102	203	1	64.2	40.75	2078	145.59
105	[73]	GFRP	150	300	0.3	36.3	2.33	583	46
106	[73]	GFRP	150	300	0.3	36.3	2.33	583	41.2
107	[73]	GFRP	150	300	0.6	36.3	4.67	584	60.52
108	[73]	GFRP	150	300	0.6	36.3	4.67	584	59.23
109	[73]	GFRP	150	300	0.6	36.3	4.67	584	59.77
110	[73]	GFRP	150	300	0.6	36.3	4.67	584	60.16
111	[73]	GFRP	150	300	0.6	36.3	4.67	584	69.02
112	[73]	GFRP	150	300	0.6	36.3	4.67	584	55.75
113	[73]	GFRP	150	300	0.6	36.3	4.67	584	56.41
114	[73]	GFRP	150	300	1.2	36.3	9.33	583	84.88
115	[73]	GFRP	150	300	1.2	36.3	9.33	583	84.33
116	[73]	GFRP	150	300	1.2	36.3	9.33	583	79.64
117	[73]	AFRP	150	300	2.4	36.3	18.67	583	106.87
118	[73]	AFRP	150	300	2.4	36.3	18.67	583	104.94
119	[73]	AFRP	150	300	2.4	36.3	18.67	583	107.91
120	[67]	CFRP	51	102	0.089	41	12.22	3501	86

Table A1. *Cont.*

No.	Ref.	Fiber Type	d (mm)	L (mm)	t (mm)	f'_{co} (MPa)	f_l (MPa)	f_f (MPa)	f'_{cc} (MPa)
121	[67]	CFRP	51	102	0.179	41	24.57	3500	120.5
122	[67]	CFRP	51	102	0.344	41	47.22	3500	158.4
123	[67]	CFRP	51	102	0.689	41	94.57	3500	241
124	[67]	CFRP	51	102	0.179	103	24.57	3500	131.1
125	[67]	CFRP	51	102	0.344	103	47.22	3500	193.2
126	[67]	CFRP	51	102	0.689	103	94.57	3500	303.6
127	[74]	CFRP	153	305	0.36	39.7	5.98	1271	55.98
128	[78]	CFRP	100	200	0.1675	30.2	9.14	2728	46.6
129	[78]	CFRP	100	200	0.5025	30.2	27.42	2728	87.2
130	[78]	CFRP	100	200	0.67	30.2	36.56	2728	104.6
131	[78]	CFRP	100	200	0.14	30.2	4.38	1564	41.7
132	[78]	CFRP	100	200	0.28	30.2	8.75	1563	56
133	[78]	CFRP	100	200	0.42	30.2	13.13	1563	63.3
134	[78]	AFRP	100	200	0.145	30.2	7.7	2655	39
135	[78]	AFRP	100	200	0.29	30.2	15.39	2653	68.5
136	[78]	AFRP	100	200	0.435	30.2	23.09	2654	92.1
137	[72]	CFRP	150	300	0.11	45.2	5.11	3484	59.4
138	[72]	CFRP	150	300	0.22	45.2	10.21	3481	79.4
139	[72]	CFRP	150	300	0.11	31.2	5.11	3484	52.4
140	[72]	CFRP	150	300	0.22	31.2	10.21	3481	67.4
141	[72]	CFRP	150	300	0.33	31.2	15.32	3482	81.7
142	[72]	CFRP	100	200	0.11	51.9	7.66	3482	75.2
143	[72]	CFRP	100	200	0.22	51.9	15.32	3482	104.6
144	[72]	CFRP	100	200	0.11	33.7	7.66	3482	69.6
145	[72]	CFRP	100	200	0.22	33.7	15.32	3482	88
146	[72]	CFRP	150	300	0.11	45.2	5.11	3484	59.4
147	[60]	CFRP	100	200	0.167	34.3	12.76	3820	57.4
148	[60]	CFRP	100	200	0.167	34.3	12.76	3820	64.9
149	[60]	CFRP	100	200	0.167	32.3	12.76	3820	58.2
150	[60]	CFRP	100	200	0.167	32.3	12.76	3820	61.8
151	[60]	CFRP	100	200	0.167	32.3	12.76	3820	57.7
152	[60]	CFRP	100	200	0.334	32.3	25.52	3820	58.2
153	[60]	CFRP	100	200	0.334	32.3	25.52	3820	61.8
154	[60]	CFRP	100	200	0.334	32.3	25.52	3820	80.2
155	[60]	CFRP	100	200	0.501	32.3	38.28	3820	86.9
156	[60]	CFRP	100	200	0.501	32.3	38.28	3820	90.1
157	[60]	CFRP	100	200	0.167	34.8	12.76	3820	57.8
158	[60]	CFRP	100	200	0.167	34.8	12.76	3820	55.6
159	[60]	CFRP	100	200	0.167	34.8	12.76	3820	50.7
160	[60]	CFRP	100	200	0.334	34.8	25.52	3820	82.7
161	[60]	CFRP	100	200	0.334	34.8	25.52	3820	81.4
162	[60]	CFRP	100	200	0.501	34.8	38.28	3820	103.3
163	[60]	CFRP	100	200	0.501	34.8	38.28	3820	110.1
164	[58]	GFRP	76	305	0.236	30.93	9.43	1518	60.82
165	[58]	CFRP	76	305	0.22	30.93	20.18	3486	95.02
166	[58]	CFRP	76	305	0.33	30.93	25.53	2940	94.01
167	[69]	CFRP	150	300	0.117	34.9	4.06	2603	46.1
168	[69]	CFRP	150	300	0.235	34.9	3.45	1101	45.8
169	[77]	CFRP	153	305	0.36	19.4	10.74	2282	33.8
170	[77]	CFRP	153	305	0.66	19.4	19.69	2282	46.4
171	[77]	CFRP	153	305	0.9	19.4	26.85	2282	62.6
172	[77]	CFRP	153	305	1.08	19.4	32.22	2282	75.7
173	[77]	CFRP	153	305	1.25	19.4	37.3	2283	80.2
174	[77]	CFRP	153	305	0.36	49	10.74	2282	59.1
175	[77]	CFRP	153	305	0.66	49	19.69	2282	76.5
176	[77]	CFRP	153	305	0.9	49	26.85	2282	98.8
177	[77]	CFRP	153	305	1.08	49	32.22	2282	112.7
178	[75]	CFRP	100	200	0.6	42	15.18	1265	73.5
179	[75]	CFRP	100	200	0.6	42	15.18	1265	73.5
180	[75]	CFRP	100	200	0.6	42	15.18	1265	67.62

Table A1. *Cont.*

No.	Ref.	Fiber Type	d (mm)	L (mm)	t (mm)	f'_{co} (MPa)	f_l (MPa)	f_f (MPa)	f'_{cc} (MPa)
181	[75]	AFRP	150	300	1.26	43	3.86	230	47.3
182	[75]	AFRP	150	300	2.52	43	7.73	230	58.91
183	[75]	AFRP	150	300	3.78	43	11.59	230	70.95
184	[75]	AFRP	150	300	5.04	43	15.46	230	74.39
185	[70]	GFRP	100	200	0.35	32	10.64	1520	54
186	[70]	GFRP	100	200	0.35	32	10.64	1520	48
187	[70]	GFRP	100	200	0.35	32	10.64	1520	54
188	[70]	GFRP	100	200	0.35	32	10.64	1520	50
189	[70]	CFRP	100	200	0.16	37	12.13	3791	60
190	[70]	CFRP	100	200	0.16	37	12.13	3791	62
191	[70]	CFRP	100	200	0.16	37	12.13	3791	59
192	[70]	CFRP	100	200	0.16	37	12.13	3791	57
193	[76]	CFRP	150	300	0.169	25.15	4.56	2024	44.13
194	[76]	CFRP	150	300	0.169	25.15	4.56	2024	41.56
195	[76]	CFRP	150	300	0.169	25.15	4.56	2024	38.75
196	[76]	CFRP	150	300	0.338	25.15	9.12	2024	60.09
197	[76]	CFRP	150	300	0.338	25.15	9.12	2024	55.93
198	[76]	CFRP	150	300	0.338	25.15	9.12	2024	61.61
199	[76]	CFRP	150	300	0.507	25.15	13.68	2024	67
200	[76]	CFRP	150	300	0.507	25.15	13.68	2024	67.27
201	[76]	CFRP	150	300	0.507	25.15	13.68	2024	70.18
202	[76]	CFRP	150	300	0.169	47.44	4.56	2024	72.26
203	[76]	CFRP	150	300	0.169	47.44	4.56	2024	64.4
204	[76]	CFRP	150	300	0.169	47.44	4.56	2024	66.19
205	[76]	CFRP	150	300	0.338	47.44	9.12	2024	82.36
206	[76]	CFRP	150	300	0.338	47.44	9.12	2024	82.35
207	[76]	CFRP	150	300	0.338	47.44	9.12	2024	79.11
208	[76]	CFRP	150	300	0.507	47.44	13.68	2024	96.29
209	[76]	CFRP	150	300	0.507	47.44	13.68	2024	95.22
210	[76]	CFRP	150	300	0.507	47.44	13.68	2024	103.97
211	[76]	CFRP	150	300	0.169	51.84	4.56	2024	78.65
212	[76]	CFRP	150	300	0.169	51.84	4.56	2024	79.18
213	[76]	CFRP	150	300	0.169	51.84	4.56	2024	72.76
214	[76]	CFRP	150	300	0.338	51.84	9.12	2024	95.4
215	[76]	CFRP	150	300	0.338	51.84	9.12	2024	90.3
216	[76]	CFRP	150	300	0.338	51.84	9.12	2024	90.65
217	[76]	CFRP	150	300	0.507	51.84	13.68	2024	110.54
218	[76]	CFRP	150	300	0.507	51.84	13.68	2024	103.62
219	[76]	CFRP	150	300	0.507	51.84	13.68	2024	117.23
220	[76]	CFRP	150	300	0.845	51.84	22.8	2024	112.66
221	[76]	CFRP	150	300	0.845	51.84	22.8	2024	126.69
222	[76]	CFRP	150	300	0.845	51.84	22.8	2024	137.93
223	[76]	CFRP	150	300	0.169	70.48	4.56	2024	87.29
224	[76]	CFRP	150	300	0.169	70.48	4.56	2024	84.03
225	[76]	CFRP	150	300	0.169	70.48	4.56	2024	83.22
226	[76]	CFRP	150	300	0.338	70.48	9.12	2024	94.06
227	[76]	CFRP	150	300	0.338	70.48	9.12	2024	98.13
228	[76]	CFRP	150	300	0.338	70.48	9.12	2024	107.2
229	[76]	CFRP	150	300	0.507	70.48	13.68	2024	114.12
230	[76]	CFRP	150	300	0.507	70.48	13.68	2024	108.07
231	[76]	CFRP	150	300	0.507	70.48	13.68	2024	110.38
232	[76]	CFRP	150	300	0.169	82.13	4.56	2024	94.08
233	[76]	CFRP	150	300	0.169	82.13	4.56	2024	97.6
234	[76]	CFRP	150	300	0.169	82.13	4.56	2024	95.83
235	[76]	CFRP	150	300	0.338	82.13	9.12	2024	97.43
236	[76]	CFRP	150	300	0.338	82.13	9.12	2024	98.85
237	[76]	CFRP	150	300	0.338	82.13	9.12	2024	98.24
238	[76]	CFRP	150	300	0.507	82.13	13.68	2024	124.2
239	[76]	CFRP	150	300	0.507	82.13	13.68	2024	129.58
240	[76]	CFRP	150	300	0.507	82.13	13.68	2024	120.36

Table A1. *Cont.*

No.	Ref.	Fiber Type	d (mm)	L (mm)	t (mm)	f'_{co} (MPa)	f_l (MPa)	f_f (MPa)	f'_{cc} (MPa)
241	[17]	GFRP	152	435	0.8	35	4.72	448	52.8
242	[17]	GFRP	152	435	1.6	35	10.6	504	66
243	[17]	GFRP	152	435	2.4	35	17.64	559	83
244	[17]	CFRP	152	435	0.11	35	4.76	3289	55
245	[17]	CFRP	152	435	0.23	35	10.72	3542	68
246	[17]	CFRP	152	435	0.55	35	26.71	3691	97
247	[71]	GFRP	153	305	1.44	30.86	9.9	526	53.66
248	[71]	GFRP	153	305	1.44	30.86	9.9	526	56.5
249	[71]	GFRP	153	305	1.44	29.64	9.9	526	67.12
250	[71]	GFRP	153	305	1.44	29.64	9.9	526	55.29
251	[71]	GFRP	153	305	1.44	29.64	9.9	526	60.23
252	[71]	GFRP	153	305	1.44	31.97	9.9	526	59.06
253	[71]	GFRP	153	305	1.44	31.97	9.9	526	60.79
254	[71]	GFRP	153	305	2.2	30.86	16.71	581	72.92
255	[71]	GFRP	153	305	2.2	30.86	16.71	581	65.67
256	[71]	GFRP	153	305	2.2	30.86	16.71	581	77.99
257	[71]	GFRP	153	305	2.2	29.64	16.71	581	74.56
258	[71]	GFRP	153	305	2.2	29.64	16.71	581	93.02
259	[71]	GFRP	153	305	2.2	29.64	16.71	581	71.74
260	[71]	GFRP	153	305	2.2	31.97	16.71	581	77.35
261	[71]	GFRP	153	305	2.2	31.97	16.71	581	77.08
262	[71]	GFRP	153	305	2.97	30.86	24.97	643	85.72
263	[71]	GFRP	153	305	2.97	30.86	24.97	643	86.76
264	[71]	GFRP	153	305	2.97	29.64	24.97	643	86.22
265	[71]	GFRP	153	305	2.97	29.64	24.97	643	114.66
266	[71]	GFRP	153	305	2.97	29.64	24.97	643	87.44
267	[71]	GFRP	153	305	2.97	31.97	24.97	643	86.11
268	[71]	GFRP	153	305	2.97	31.97	24.97	643	83.99
269	[68]	GFRP	150	300	4.28	25.61	37.21	652	71
270	[68]	GFRP	150	300	4.28	25.61	37.21	652	71.3
271	[68]	GFRP	150	300	4.28	25.61	37.21	652	74.7
272	[68]	GFRP	150	300	4.28	25.61	37.21	652	79.2
273	[68]	GFRP	150	300	4.28	25.61	37.21	652	81.5
274	[68]	GFRP	150	300	4.28	25.61	37.21	652	77.5
275	[68]	GFRP	150	300	4.28	25.61	37.21	652	89.9
276	[68]	GFRP	150	300	5.9	25.61	52.71	670	98.5
277	[68]	GFRP	150	300	5.9	25.61	52.71	670	110.3
278	[68]	GFRP	150	300	5.9	25.61	52.71	670	105.2
279	[66]	GFRP	168	336	3.73	58	24.33	548	90
280	[66]	GFRP	219	438	3.7	58	18.52	548	68
281	[66]	GFRP	100	200	3.08	37	24.52	398	81

References

1. Kamgar, R.; Bagherinejad, M.H.; Heidarzadeh, H. A new formulation for prediction of the shear capacity of FRP in strengthened reinforced concrete beams. *Soft Comput.* **2019**. [CrossRef]
2. Wu, H.C.; Eamon, C.D. *Strengthening of Concrete Structures Using Fiber Reinforced Polymers (FRP): Design, Construction and Practical Applications*; Woodhead Publishing: Cambridge, MA, USA, 2017.
3. De Lorenzis, L.; Tepfers, R. Comparative study of models on confinement of concrete cylinders with fiber-reinforced polymer composites. *J. Compos. Constr.* **2003**, *7*, 219–237. [CrossRef]
4. Colomb, F.; Tobbi, H.; Ferrier, E.; Hamelin, P. Seismic retrofit of reinforced concrete short columns by CFRP materials. *Compos. Struct.* **2008**, *82*, 475–487. [CrossRef]
5. Niroomandi, A.; Maheri, A.; Maheri, M.R.; Mahini, S.S. Seismic performance of ordinary RC frames retrofitted at joints by FRP sheets. *Eng. Struct.* **2010**, *32*, 2326–2336. [CrossRef]
6. Ozcan, O.; Binici, B.; Ozcebe, G. Improving seismic performance of deficient reinforced concrete columns using carbon fiber-reinforced polymers. *Eng. Struct.* **2008**, *30*, 1632–1646. [CrossRef]
7. Promis, G.; Ferrier, E.; Hamelin, P. Effect of external FRP retrofitting on reinforced concrete short columns for seismic strengthening. *Compos. Struct.* **2009**, *88*, 367–379. [CrossRef]

8. Satasivam, S.; Bai, Y. Mechanical performance of modular FRP-steel composite beams for building construction. *Mater. Struct.* **2016**, *49*, 4113–4129. [CrossRef]
9. Shateri, M.; Ghaib, M.; Svecova, D.; Thomson, D. On acoustic emission for damage detection and failure prediction in fiber reinforced polymer rods using pattern recognition analysis. *Smart Mater. Struct.* **2017**, *26*, 065023. [CrossRef]
10. Zafar, A.; Andrawes, B. Incremental dynamic analysis of concrete moment resisting frames reinforced with shape memory composite bars. *Smart Mater. Struct.* **2012**, *21*, 025013. [CrossRef]
11. Cevik, A. Modeling strength enhancement of FRP confined concrete cylinders using soft computing. *Expert Syst. Appl.* **2011**, *38*, 5662–5673. [CrossRef]
12. Berthet, J.; Ferrier, E.; Hamelin, P. Compressive behavior of concrete externally confined by composite jackets: Part B: Modeling. *Constr. Build. Mater.* **2006**, *20*, 338–347. [CrossRef]
13. Lam, L.; Teng, J. Strength models for fiber-reinforced plastic-confined concrete. *J. Struct. Eng.* **2002**, *128*, 612–623. [CrossRef]
14. Li, Y.F.; Lin, C.T.; Sung, Y.Y. A constitutive model for concrete confined with carbon fiber reinforced plastics. *Mech. Mater.* **2003**, *35*, 603–619. [CrossRef]
15. Matthys, S.; Toutanji, H.; Audenaert, K.; Taerwe, L. Axial load behavior of large-scale columns confined with fiber-reinforced polymer composites. *ACI Struct. J.* **2005**, *102*, 258.
16. Miyauchi, K.; Inoue, S.; Kuroda, T.; Kobayashi, A. Strengthening effects of concrete column with carbon fiber sheet. *Trans. Jpn. Concr. Inst.* **2000**, *21*, 143–150.
17. Saafi, M.; Toutanji, H.; Li, Z. Behavior of concrete columns confined with fiber reinforced polymer tubes. *Mater. J.* **1999**, *96*, 500–509.
18. Vintzileou, E.; Panagiotidou, E. An empirical model for predicting the mechanical properties of FRP-confined concrete. *Constr. Build. Mater.* **2008**, *22*, 841–854. [CrossRef]
19. Xiao, Y.; Wu, H. Compressive behavior of concrete confined by carbon fiber composite jackets. *J. Mater. Civ. Eng.* **2000**, *12*, 139–146. [CrossRef]
20. Richart, F.E.; Brandtzaeg, A.; Brown, R.L. *A Study of the Failure of Concrete under Combined Compressive Stresses*; Bulletin No. 185; University of Illinois at Urbana Champaign, College of Engineering, Engineering Experimental Station: Champaign, IL, USA, 1928.
21. Cevik, A.; Cabalar, A.F. A genetic-programming-based formulation for the strength enhancement of fiber-reinforced-polymer-confined concrete cylinders. *J. Appl. Polym. Sci.* **2008**, *110*, 3087–3095. [CrossRef]
22. Cevik, A.; Göğüş, M.T.; Güzelbey, İ.H.; Filiz, H. Soft computing based formulation for strength enhancement of CFRP confined concrete cylinders. *Adv. Eng. Softw.* **2010**, *41*, 527–536. [CrossRef]
23. Cevik, A.; Guzelbey, I.H. Neural network modeling of strength enhancement for CFRP confined concrete cylinders. *Build. Environ.* **2008**, *43*, 751–763. [CrossRef]
24. Elsanadedy, H.M.; Al-Salloum, Y.A.; Abbas, H.; Alsayed, S.H. Prediction of strength parameters of FRP-confined concrete. *Compos. Part B Eng.* **2012**, *43*, 228–239. [CrossRef]
25. Mohammad Rezapour Tabari, M.; Nasr Azadani, M.; Kamgar, R. Development of operation multi-objective model of dam reservoir under conditions of temperature variation and loading using NSGA-II and DANN models: A case study of Karaj /Amir Kabir dam. *Soft Comput.* **2020**. [CrossRef]
26. Ghaleini, E.N.; Koopialipoor, M.; Momenzadeh, M.; Sarafraz, M.E.; Mohamad, E.T.; Gordan, B. A combination of artificial bee colony and neural network for approximating the safety factor of retaining walls. *Eng. Comput.* **2019**, *35*, 647–658. [CrossRef]
27. Hüsken, M.; Jin, Y.; Sendhoff, B. Structure optimization of neural networks for evolutionary design optimization. *Soft Comput.* **2005**, *9*, 21–28. [CrossRef]
28. Jalal, M.; Ramezanianpour, A.A. Strength enhancement modeling of concrete cylinders confined with CFRP composites using artificial neural networks. *Compos. Part B Eng.* **2012**, *43*, 2990–3000. [CrossRef]
29. Kamgar, R.; Hatefi, S.M.; Majidi, N. A fuzzy inference system in constructional engineering projects to evaluate the design codes for RC buildings. *Civ. Eng. J.* **2018**, *4*, 2155–2172. [CrossRef]
30. Keshtegar, B.; Ozbakkaloglu, T.; Gholampour, A. Modeling the behavior of FRP-confined concrete using dynamic harmony search algorithm. *Eng. Comput.* **2017**, *33*, 415–430. [CrossRef]
31. Moosazadeh, S.; Namazi, E.; Aghababaei, H.; Marto, A.; Mohamad, H.; Hajihassani, M. Prediction of building damage induced by tunnelling through an optimized artificial neural network. *Eng. Comput.* **2019**, *35*, 579–591. [CrossRef]

32. Najafzadeh, M.; Azamathulla, H.M. Neuro-fuzzy GMDH to predict the scour pile groups due to waves. *J. Comput. Civ. Eng.* **2013**, *29*, 04014068. [CrossRef]
33. Najafzadeh, M.; Etemad-Shahidi, A.; Lim, S.Y. Scour prediction in long contractions using ANFIS and SVM. *Ocean Eng.* **2016**, *111*, 128–135. [CrossRef]
34. Najafzadeh, M.; Lim, S.Y. Application of improved neuro-fuzzy GMDH to predict scour depth at sluice gates. *Earth Sci. Inform.* **2015**, *8*, 187–196. [CrossRef]
35. Najafzadeh, M.; Sattar, A.M. Neuro-fuzzy GMDH approach to predict longitudinal dispersion in water networks. *Water Resour. Manag.* **2015**, *29*, 2205–2219. [CrossRef]
36. Najafzadeh, M.; Tafarojnoruz, A. Evaluation of neuro-fuzzy GMDH-based particle swarm optimization to predict longitudinal dispersion coefficient in rivers. *Environ. Earth Sci.* **2016**, *75*, 157–169. [CrossRef]
37. Siemaszko, A.; Jakubczyk-Gałczyńska, A.; Jankowski, R. The idea of using Bayesian networks in forecasting impact of traffic-induced vibrations transmitted through the ground on residential buildings. *Geosciences* **2019**, *9*, 339. [CrossRef]
38. Khatami, S.M.; Naderpour, H.; Barros, R.C.; Jakubczyk-Gałczyńska, A.; Jankowski, R. Effective formula for impact damping ratio for simulation of earthquake-induced structural pounding. *Geosciences* **2019**, *9*, 347. [CrossRef]
39. Khatami, S.M.; Naderpour, H.; Barros, R.C.; Jakubczyk-Gałczyńska, A.; Jankowski, R. Determination of peak impact force for buildings exposed to structural pounding during earthquakes. *Geosciences* **2020**, *10*, 18. [CrossRef]
40. Kamgar, R.; Gholami, F.; Zarif Sanayei, H.R.; Heidarzadeh, H. Modified tuned liquid dampers for seismic protection of buildings considering soil-structure interaction effects. *Iran. J. Sci. Technol. Trans. Civ. Eng.* **2020**, *44*, 339–354. [CrossRef]
41. Kamgar, R.; Askari Dolatabad, Y.; Babadaei Samani, M.R. Seismic optimization of steel shear wall using shape memory alloy. *Int. J. Optim. Civ. Eng.* **2019**, *9*, 671–687.
42. Lee, S.; Lee, C. Prediction of shear strength of FRP-reinforced concrete flexural members without stirrups using artificial neural networks. *Eng. Struct.* **2014**, *61*, 99–112. [CrossRef]
43. Sobhani, J.; Najimi, M.; Pourkhorshidi, A.R.; Parhizkar, T. Prediction of the compressive strength of no-slump concrete: A comparative study of regression, neural network and ANFIS models. *Constr. Build. Mater.* **2010**, *24*, 709–718. [CrossRef]
44. Cheng, M.Y.; Cao, M.T. Evolutionary multivariate adaptive regression splines for estimating shear strength in reinforced-concrete deep beams. *Eng. Appl. Artif. Intell.* **2014**, *28*, 86–96. [CrossRef]
45. Behnood, A.; Olek, J.; Glinicki, M.A. Predicting modulus elasticity of recycled aggregate concrete using M5′ model tree algorithm. *Constr. Build. Mater.* **2015**, *94*, 137–147. [CrossRef]
46. Ebrahimpour Komleh, H.; Maghsoudi, A.A. Prediction of curvature ductility factor for FRP strengthened RHSC beams using ANFIS and regression models. *Comput. Concr.* **2015**, *16*, 399–414. [CrossRef]
47. Gu, Z.Q.; Oyadiji, S.O. Application of MR damper in structural control using ANFIS method. *Comput. Struct.* **2008**, *86*, 427–436. [CrossRef]
48. Amani, J.; Moeini, R. Prediction of shear strength of reinforced concrete beams using adaptive neuro-fuzzy inference system and artificial neural network. *Sci. Iran.* **2012**, *19*, 242–248. [CrossRef]
49. Mashrei, M.A.; Seracino, R.; Rahman, M. Application of artificial neural networks to predict the bond strength of FRP-to-concrete joints. *Constr. Build. Mater.* **2013**, *40*, 812–821. [CrossRef]
50. Mohammadhassani, M.; Nezamabadi-Pour, H.; Jumaat, M.; Jameel, M.; Hakim, S.J.S.; Zargar, M. Application of the ANFIS model in deflection prediction of concrete deep beam. *Struct. Eng. Mech.* **2013**, *45*, 319–332. [CrossRef]
51. Nehdi, M.; Nikopour, H. Genetic algorithm model for shear capacity of RC beams reinforced with externally bonded FRP. *Mater. Struct.* **2011**, *44*, 1249–1258. [CrossRef]
52. Li, Y.L.; Teng, J.G.; Zhao, X.L.; Singh Raman, R.K. Theoretical model for seawater and sea sand concrete-filled circular FRP tubular stub columns under axial compression. *Eng. Struct.* **2018**, *160*, 71–84. [CrossRef]
53. Li, P.; Wu, Y.F.; Gravina, R. Cyclic response of FRP-confined concrete with post-peak strain softening behavior. *Constr. Build. Mater.* **2016**, *123*, 814–828. [CrossRef]
54. Zhou, A.; Qin, R.; Chow, C.L.; Lau, D. Structural performance of FRP confined seawater concrete columns under chloride environment. *Compos. Struct.* **2019**, *216*, 12–19. [CrossRef]

55. Mansouri, I.; Ozbakkaloglu, T.; Kisi, O.; Xie, T. Predicting behavior of FRP-confined concrete using neuro-fuzzy, neural network, multivariate adaptive regression splines and M5 model tree techniques. *Mater. Struct.* **2016**, *49*, 4319–4334. [CrossRef]
56. Naderpour, H.; Kheyroddin, A.; Amiri, G.G. Prediction of FRP-confined compressive strength of concrete using artificial neural networks. *Compos. Struct.* **2010**, *92*, 2817–2829. [CrossRef]
57. Spoelstra, M.R.; Monti, G. FRP-confined concrete model. *J. Compos. Constr.* **1999**, *3*, 143–150. [CrossRef]
58. Toutanji, H. Stress-strain characteristics of concrete columns externally confined with advanced fiber composite sheets. *Mater. J.* **1999**, *96*, 397–404.
59. Samaan, M.; Mirmiran, A.; Shahawy, M. Model of concrete confined by fiber composites. *J. Struct. Eng.* **1998**, *124*, 1025–1031. [CrossRef]
60. Kono, S.; Inazumi, M.; Kaku, T. Evaluation of confining effects of CFRP sheets on reinforced concrete members. In Proceedings of the Second International Conference on Composites in Infrastructure National Science Foundation, Tucson, AZ, USA, 5–7 January 1998.
61. Karbhari, V.M.; Gao, Y. Composite jacketed concrete under uniaxial compression-Verification of simple design equations. *J. Mater. Civ. Eng.* **1997**, *9*, 185–193. [CrossRef]
62. Mander, J.B.; Priestley, M.J.; Park, R. Theoretical stress-strain model for confined concrete. *J. Struct. Eng.* **1988**, *114*, 1804–1826. [CrossRef]
63. Fardis, M.N.; Khalili, H. Concrete encased in fiberglass-reinforced plastic. *J. Am. Concr. Inst.* **1981**, *78*, 440–446.
64. Fardis, M.N.; Khalili, H.H. FRP-encased concrete as a structural material. *Mag. Concr. Res.* **1982**, *34*, 191–202. [CrossRef]
65. Ahmad, S.; Khaloot, A.; Irshaid, A. Behaviour of concrete spirally confined by fibreglass filaments. *Mag. Concr. Res.* **1991**, *43*, 143–148. [CrossRef]
66. Fam, A.Z.; Rizkalla, S.H. Concrete-filled FRP tubes for flexural and axial compression members. In Proceedings of the Third International Conference on Advanced Composite Materials in Bridges and Structures, Ottawa, ON, Canada, 15–18 August 2000.
67. Harmon, T.G.; Slattery, K.T. Advanced composite confinement of concrete. In Proceedings of the First International Conference on Advanced Composite Materials in Bridges and Structures, Sherbrooke, QC, Canada, 7–9 October 1992.
68. La Tegola, A.; Manni, O. Experimental investigation on concrete confined by fiber reinforced polymer and comparison with theoretical model. *Spec. Publ.* **1999**, *188*, 243–254.
69. Matthys, S.; Taerwe, L.; Audenaert, K. Tests on axially loaded concrete columns confined by fiber reinforced polymer sheet wrapping. *Spec. Publ.* **1999**, *188*, 217–228.
70. Micelli, F.; Myers, J.; Murthy, S. Effect of environmental cycles on concrete cylinders confined with FRP. In Proceedings of the CCC2001 International Conference on Composites in Construction, Porto, Portugal, 10–12 October 2001.
71. Mirmiran, A.; Shahawy, M. Behavior of concrete columns confined by fiber composites. *J. Struct. Eng.* **1997**, *123*, 583–590. [CrossRef]
72. Miyauchi, K. Estimation of strengthening effects with carbon fiber sheet for concrete column. In Proceedings of the 3rd International Symposium on Non-Metallic (FRP) Reinforcement for Concrete Structures, Sapporo, Japan, 14–16 October 1997.
73. Nanni, A.; Bradford, N.M. FRP jacketed concrete under uniaxial compression. *Constr. Build. Mater.* **1995**, *9*, 115–124. [CrossRef]
74. Picher, F.; Rochette, P.; Labossiére, P. Confinement of concrete cylinders with CFRP. In Proceedings of the International Conference on Composites in Infrastructure, Tuscon, AZ, USA, 15–17 January 1996.
75. Rochette, P.; Labossiere, P. Axial testing of rectangular column models confined with composites. *J. Compos. Constr.* **2000**, *4*, 129–136. [CrossRef]
76. Rousakis, T.; Tepfers, R. *Experimental Investigation of Concrete Cylinders Confined by Carbon FRP Sheets, under Monotonic and Cyclic Axial Compressive Load*; Chalmers University of Technology: Goteborg, Sweden, 2001.
77. Shahawy, M.; Mirmiran, A.; Beitelman, T. Tests and modeling of carbon-wrapped concrete columns. *Compos. Part B Eng.* **2000**, *31*, 471–480. [CrossRef]

78. Watanabe, K.; Nakamura, H.; Honda, Y.; Toyoshima, M. Confinement effect of FRP sheet on strength and ductility of concrete cylinders under uniaxial compression. In Proceedings of the Third International Symposium (FRPRCS-3) on Non-Metallic (FRP) Reinforcement for Concrete Structures, Sapporo, Japan, 14–16 October 1997; pp. 233–240.
79. Rojas, R. *Neural Networks: A Systematic Introduction*; Springer: Berlin/Heidelberg, Germany, 2013.
80. Dehkordi, A.N.; Kamali-Asl, A.; Wen, N.; Mikkelsen, T.; Chetty, I.J.; Bagher-Ebadian, H. DCE-MRI prediction of survival time for patients with glioblastoma multiforme: Using an adaptive neuro-fuzzy-based model and nested model selection technique. *NMR Biomed.* **2017**, *30*, e3739. [CrossRef]
81. Huang, X. *Study on ANN Noise Adaptability in Application of Industry Process Characteristics Mining*; Advanced Materials Research; Trans Tech Publications Ltd.: Stafa Zurich, Switzerland, 2012; Volume 462, pp. 635–640.